JOURNAL OF PROPULSION AND POWER
Vol. 23, No. 1, January–February 2007

Combustion Stability Boundaries of the Subscale Rocket Chamber with Impinging Jet Injectors

Chae Hoon Sohn*
Chosun University, Gwangju 501-759, Republic of Korea
Woo Seok Seol†
Korea Aerospace Research Institute, Daejeon 305-333, Republic of Korea
and
Alexander A. Shibanov‡ and Valery P. Pikalov§
Research Institute of Chemical Machine Building (NIICHIMMASH), 141300, Sergiev Posad, Russia

DOI: 10.2514/1.19937

Combustion stability boundaries are investigated experimentally using a subscale chamber for screening the split-triplet impinging jet injectors of a liquid propellant rocket engine. Geometrical dimensions and operating conditions of the subscale chamber are determined using the scaling methods proposed in the previous works. From the experimental tests, two major instability regions are identified by the parameters of combustion-chamber pressure and mixture (oxidizer/fuel) ratio. A key instability mechanism can be explained by the correlation between the characteristic burning or mixing time and the characteristic acoustic time. In each instability region, the dynamic behavior of the flame is investigated to verify the characteristic lengths of the jet injectors derived from hydrodynamic theory. It is found that pressure oscillations with large amplitude are generated by lifted-off flames. Stability margins are evaluated as a function of the impingement angle and thereby, the optimum angle is identified.

Nomenclature

A	=	amplitude of pressure oscillation
A_{th}	=	nozzle throat area of the actual combustion chamber
C	=	sound speed
c^*	=	characteristic exhaust velocity
D	=	diameter of the chamber
d	=	diameter of the injector orifice
F	=	fuel
f	=	frequency
f_1, f_2	=	frequencies at which the pressure amplitude corresponds to $p_{\text{peak}}/\sqrt{2}$ on amplitude spectrum ($f_2 > f_1$)
K_m	=	mixture ratio, $\equiv \dot{m}_O/\dot{m}_F$
L	=	length of the chamber or the length of the entire combustion zone
l	=	length
M	=	Mach number
$\dot{m}$	=	mass flow rate
n_{inj}	=	number of injectors
O	=	oxidizer
p	=	pressure
q	=	square root of oxidizer/fuel jet dynamic-head ratio, $\equiv U_O/U_F\sqrt{\rho_O/\rho_F}$
$\bar{R}$	=	stability margin defined in Eq. (2)
T	=	acoustic oscillation period
U	=	propellant injection velocity
α	=	impingement angle of the injector
η	=	damping factor, $\equiv (f_2 - f_1)/f_{\text{peak}}$
Λ_O	=	characteristic length of disturbance wave propagating along the oxidizer jet, $\equiv U_O/f_{\text{ch}} = U_O T$
ρ	=	density
τ	=	characteristic time

Subscripts

a	=	actual (full-scale) combustion chamber
chem	=	chemical reaction
ch	=	combustion chamber
cz	=	combustion zone
des	=	design operating condition
F	=	fuel
inj	=	injector
max	=	maximum value
min	=	minimum value
mix	=	mixing
O	=	oxidizer
peak	=	peak response
s	=	subscale combustion chamber
stab	=	flame stabilization point
tot	=	total
1T	=	the first tangential acoustic mode
1T1L	=	the combined acoustic mode of the first tangential and the first longitudinal modes

Received 7 September 2005; accepted for publication 16 March 2006.

*Assistant Professor, Department of Aerospace Engineering; chsohn@chosun.ac.kr. Member AIAA.
†Head, Rocket Engine Department. Member AIAA.
‡Senior Research Engineer, Research Department.
§Head, Research Department.

I. Introduction

HIGH-frequency combustion instability is the phenomenon of amplification of pressure oscillations through in-phase heat addition/extraction from combustion. It is often called acoustic instability and is of significant interest in propulsion and power systems. It can lead to undesired intense pressure fluctuations as well as excessive heat transfer to the combustor wall in combustion systems such as solid and liquid propellant rocket engines, ramjets, turbojet thrust augmentors, utility boilers, and furnaces [1–3]. For a long time, it has caused common problems in the course of rocket-engine development, i.e., thermal damage on the injector faceplate and the combustor wall, severe mechanical vibration of the rocket body, unpredictable malfunction of engines, etc.

Combustion-instability mechanisms are rather complex, involving many processes such as injection, atomization, vaporization, mixing, and chemical kinetics, and only limited information is available to predict the occurrence of combustion instability although a number of works have focused on the issue. Extensive reviews of the individual processes affecting combustion instability can be found in the literature [4,5] and in the references therein. As one noticeable example, an empirical stability correlation for like-on-like injectors has been presented, where the stability boundaries of various rocket engines were correlated in terms of the acoustic frequency and the injector operating condition, i.e., the ratio of oxidizer jet velocity to orifice diameter. The correlation has shown that the lowest sustainable stability frequency is linearly proportional to this ratio [4–7]. However, there are many possible injector configurations (e.g., like-on-like doublets, unlike doublets, triplets, etc.) and a generalized correlation applicable to any configuration has not been proposed. Besides, there is still no definite or conclusive proof concerning the mechanisms of instability [4]. Most of the works focused on this issue suggest that many processes interact in a complex manner in triggering instability. Accordingly, the specific mechanism may have to be pursued in the specific system.

In the development of new rocket combustor, combustion stability is one of the design factors that should be checked by engine designers. As mentioned, because a number of processes are involved in the reactive flowfield in the combustion chamber, there are various hardware devices affecting combustion instability. Out of them, the injector is the most important in establishing the combustion field because it controls the injection, atomization, and mixing of the propellants. Therefore, the impact of candidate injectors on combustion stability needs to be examined for injector screening at the initial stage of combustor development to select a suitable injector configuration. The most reliable method is to conduct experimental tests using actual (full-scale) rocket motors [8,9] and combustion chambers with candidate injectors [10], which is expensive both in experimental cost and time. It is necessary to find a cost-effective way without losing its essential characteristics. One method is to use a subscale chamber instead of the actual-size chamber. Fisher et al. summarized the subscale experimental techniques using various subscale combustors and the advantages and limitations of the use of each combustor [11]. Furthermore, mechanisms of combustion instability can be investigated more effectively with specific subscale combustors. The previous works [12,13] proposed a scaling method for hot-fire modeling of high-frequency combustion instability using a specific subscale chamber. In the works, general principles of modeling were described concerning the geometric and flame-condition similarities between subscale and full-scale chambers, the calculation of chamber geometry, and the scaling-up of subscale-chamber test data to actual operating conditions.

In the present study, the methods proposed in the previous studies are realized experimentally and the instability mechanism is discussed based on the experimental data. The impinging jet injectors [14–16], which are the simplest injectors and have been frequently used in the early low-thrust engines, employed in this study are the split-triplet impinging jet injectors. They tend to trigger the instability more easily than the coaxial injectors. With an emphasis on the propellant mixing processes, the exact coupling between injection dynamics and chamber acoustics, which has never been tried, is established experimentally in this work. The stability boundaries are obtained using chamber pressure and mixture (oxidizer-fuel) ratio, and the dynamic behavior of the flames is investigated in each unstable region to determine the instability mechanism. The stability margins are evaluated as a function of the impingement angle to determine the most stable injector configuration and the optimum angle.

II. Experimental Methods

A. Subscale Test Apparatus for Firing Tests

The full-scale combustion chamber under study employs split-triplet (F-O-O-F) impinging jet injectors, and the propellants are

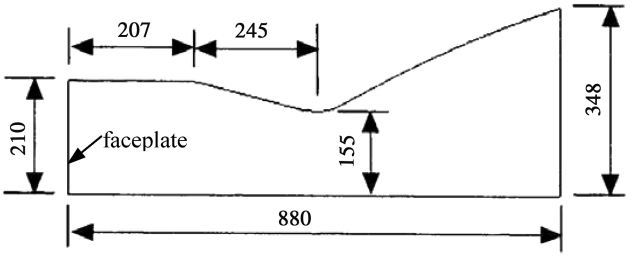

a) Geometry and dimensions of the actual combustion chamber

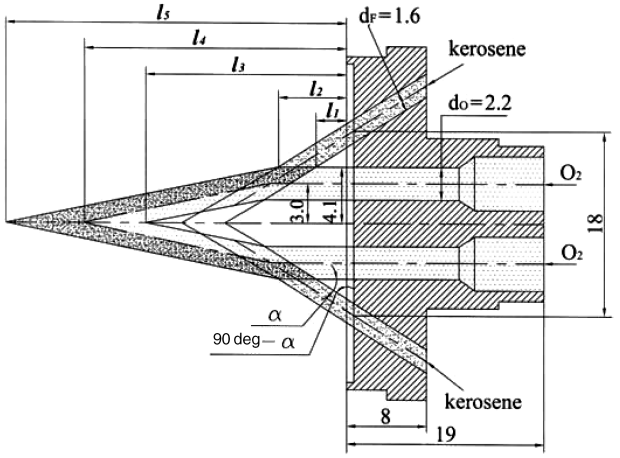

b) F-O-O-F impinging jet injector and the characteristic lengths of oxidizer and fuel jet streams

Fig. 1 Schematic diagrams of the actual combustion chamber and the configuration of the bipropellant impinging jet injector (all dimensions in mm).

kerosene and liquid oxygen. Schematic diagrams and basic geometrical dimensions of the combustion chamber and the injector are shown in Fig. 1. The nominal chamber pressure and mixture ratio are 1.4 MPa and 2.34, respectively.

A schematic diagram of the firing-test setup is shown in Fig. 2. The subscale combustion chamber has a cylindrical shape and is installed vertically (chamber-exit upwards) on a plate that simulates the injector head. A five-injector unit is mounted on the plate, so that the injector exit is flush with the plate surface. The model injector head is illustrated in Fig. 3. The combustion chamber operates at atmospheric pressure and can move freely on the injector-faceplate simulator. This arrangement allows the formation of flames at any

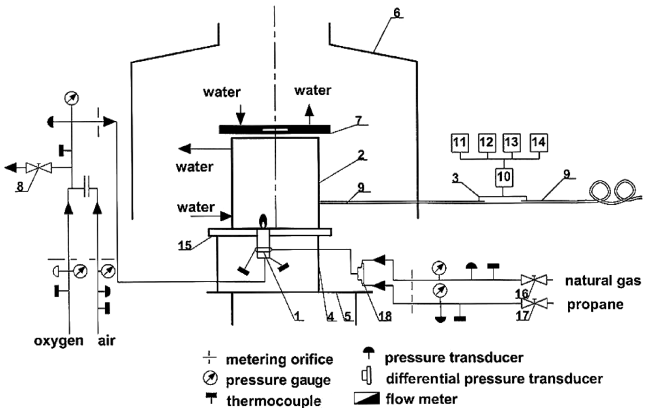

Fig. 2 Schematic diagram of hot-fire subscale test apparatus (1: injector, 2: combustion chamber, 3: pressure pulsation transducer, 4: seat, 5: table, 6: exhaust vent, 7: perforated lid, 8: throttle, 9: acoustic probe, 10: broadband amplifier, 11: oscilloscope, 12: spectrum analyzer, 13: digital voltmeter, 14: personal computer, 15: injector faceplate, 16: methane line throttle, 17: propane line throttle, 18: mixer).

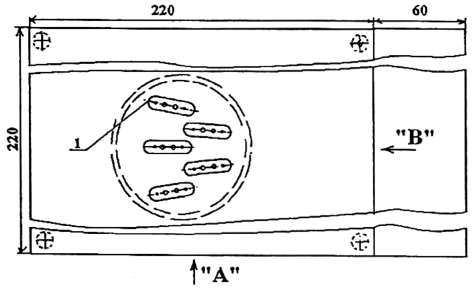

Fig. 3 Model injector head with five-element injectors viewed from the chamber exit.

point in the acoustic field, so that we may evaluate the tendency of the combustion process to excite pressure oscillations at various acoustic modes, i.e., the nth tangential and radial modes.

As discussed by Sohn et al. [13], the oxidizer and the fuel are simulated by the gaseous oxygen and the gaseous methane-propane mixture, respectively. To maintain the oxidizer to fuel density ratio equal to that of the full-scale chamber, the fuel consists of 54% methane and 46% propane by mass. Pure oxygen is supplied through the oxidizer feed line and the methane-propane mixture is supplied through the fuel feed line at room temperature. The mass flow rates of the propellants are carefully controlled with a throttling device connected to a personal computer (PC) receiving signals from pressure and temperature sensors upstream of the metering orifices. The present measurement system can measure mass flow rates with an accuracy of 2%. To measure propellant temperature directly upstream of the injector, thermocouples are installed in the oxidizer and fuel manifolds. The seat, which houses the subscale chamber with the injector unit, is mounted on a special table.

The aforementioned subscale test apparatus is used to determine the boundaries of the regions of acoustic oscillations excited at given propellant flow rates. Pressure pulsations from the combustion field in the subscale chamber are measured using an acoustic probe that consists of a coiled long metal tube with an inner diameter of 4 mm. An uncooled piezoelectric pressure transducer is installed at 320 mm from the tube inlet. It has been verified that amplitude-frequency characteristics are uniform over the frequency range from 0 to 10 kHz using the pressure transducer. Another acoustic probe is inserted into a hole in the chamber wall near the faceplate of the model injector head. The signals from the transducers are amplified by a broadband amplifier, recorded by a personal computer, and sent to visual instruments, i.e., an oscilloscope, a digital voltmeter, and a spectrum analyzer.

The evaluation of the high-frequency combustion instability is made instantaneously during the test based on the characteristics of oscillations on the oscilloscope screen and the spectral behavior of oscillations displayed on the PC screen and the spectrum analyzer. Combustion processes resulting in irregular acoustic oscillations with a broadband spectrum are considered to be stable. Combustion processes that exhibit regular oscillatory behavior, almost sinusoidal in nature, with a spectrum containing individual sharp peaks are considered to be unstable. Unstable regimes are classified into small- and medium-amplitude oscillations. As a rule, the amplitude of small-amplitude oscillations is about 3–4 times higher than the noise level, whereas the amplitude of medium-amplitude oscillations is more than 10 times the noise level.

Boundaries separating stable and unstable operating conditions are usually not so clear. To catch smooth onset of unstable combustion, the operating condition is changed minutely when determining self-excitation boundaries. The volumetric flow rates of fuel and oxidizer are equal to the actual volumetric flow rates in the full-scale combustion chamber as discussed in the previous works [12,13]. With the oxidizer and the fuel densities predetermined, the ranges of the propellant mass flow rates can be determined. The ratio of the fuel mass flow rate to the oxidizer mass flow rate is kept the same as that in the actual system. To cover the wide range of operating conditions including the nominal point, the ranges of mass flow rates under consideration are as follows: $\dot{m}_{O_2} = 0.60$–3.60 g/s, $\dot{m}_{CH_4} = 0.17$–1.00 g/s, and $\dot{m}_{C_3H_8} = 0.08$–0.48 g/s.

B. Test Procedures for Firing Tests

At first, both volumetric flow rates of fuel and oxidizer are set to their minimum values. In this initial regime, all the specified parameters are recorded and the experimental test is conducted; propellants are ignited and pressure fluctuations are measured. Assessment of the stability (stable or unstable combustion) in the regime is made on the basis of visual monitoring of the pressure pulsations. Then, the oxidizer flow rate is increased gradually up to its maximum value. An emphasis is put on the boundaries of the regimes where self-excited oscillations occur during this procedure. After that, the fuel flow rate is set to a higher value and all operations are repeated in the same manner. The basic configuration of the injector has an impingement angle of 30 deg and the others have 20, 15, and 12.5 deg.

For a comprehensive analysis of the combustion behavior at various operating conditions, the pressure oscillations for various operating regimes are recorded in the PC memory. The duration of each record is about 2–3 s. In the course of signal processing, the oscillation frequency, the amplitude, and the damping factor [17] for ten major spectral maxima are printed in tables, and the spectrograms are printed in each regime. Subscale test data are scaled-up to the actual operating conditions by the procedures described in the previous works [12,13].

C. Subscale Chamber

The method to select the geometric dimensions of the subscale combustion chamber acting as an acoustic resonator at various oscillating natural frequencies, f_{ch}, has been described in detail in the previous works [12,13]. To preserve the chamber acoustics, the geometric dimensions of the subscale chamber should be selected to provide the same natural frequencies in the subscale chamber as those in the actual full-scale chamber.

From the condition of the equality of transverse oscillation frequencies between the actual chamber and the subscale chamber, the diameter of the subscale chamber is determined by the equation [13,18,19],

$$D_{ch,s} = D_{ch,a} \frac{C_{ch,s}}{C_{ch,a}} \left(\frac{1 - M_{ch,s}^2}{1 - M_{ch,a}^2} \right)^{0.5} \tag{1}$$

where C and M denote sound speed and Mach number of the mixture of combustion products, respectively. From the previous works [10,20] and the preliminary test in the present study, the experimental data of $M_{ch,a} \approx M_{ch,s} = 0.32$, $C_{ch,a} = 1180$ m/s, and $C_{ch,s} = 470$–500 m/s were obtained. With $D_{ch,a} = 420$ mm as shown in Fig. 1a, Eq. (1) gives $D_{ch,s} = 170$–180 mm. In a similar manner, the length of the subscale chamber can be calculated to be 240–260 mm. As a result of this scaling, the actual chamber acoustics are preserved in the subscale chamber. The resonant frequencies of the two principal transverse oscillatory modes, 1T and 1T1L, are predicted to be $f_{1T} = 1560$ Hz and $f_{1T1L} \cong 2000$ Hz, respectively.

III. Results and Discussions

A. Stability Boundaries

With the injector configuration of $\alpha = 30$ deg, the measured instability-region boundaries are shown in Fig. 4 on the coordinate plane of chamber pressure vs mixture ratio. Chamber pressure is calculated using the total mass flow rate, the characteristic exhaust velocity, and the nozzle throat area as described in the previous work [13]: $p_{ch} = \dot{m}_{tot} c^* / A_{th}$. In Fig. 4, the rectangular region, the center of which indicates the nominal operating condition, shows the operating conditions of the actual rocket combustor. It is often called the operating window or range. The stability margin is defined as

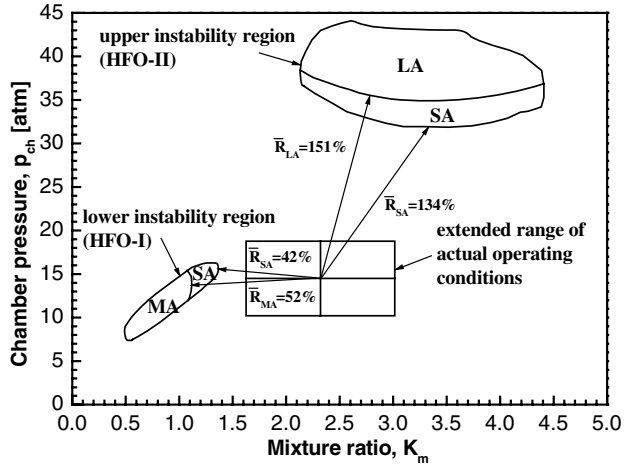

Fig. 4 Stability boundaries and margins of the injectors with the impingement angle of 30 deg plotted on the coordinate of chamber pressure vs mixture ratio (LA: large amplitude, MA: medium amplitude, and SA: small amplitude).

$$\bar{R} = \left[\left(\frac{\Delta p_{\text{ch}}}{p_{\text{ch,des}}} \right)^2 + \left(\frac{\Delta K_m}{K_{m,\text{des}}} \right)^2 \right]^{0.5} \tag{2}$$

where $\Delta p_{\text{ch}} = p_{\text{ch}} - p_{\text{ch,des}}$ and $\Delta K_m = K_m - K_{m,\text{des}}$. The normalized stability margin defined here indicates how far the unstable region is from the nominal operating condition on the p_{ch}–K_m coordinate plane.

From Fig. 4, it can be seen that the combustion process established by the present injectors causes two principal unstable regions, labeled as the lower and the upper instability regions. The lower region of high-frequency oscillations at the frequency of $f_{1T1L} = 1850 \pm 150$ Hz (denoted by the region, HFO-I) is located on the left of the actual operating range. A representative amplitude spectrum is shown in Fig. 5. The high-frequency oscillations in this region are of small or medium amplitude of about 100 kPa with damping factors of 3.9–6.5%. The spectrum of these oscillations shows one peak at a frequency of approximately 1850 Hz. The peak amplitude is higher than those at the other frequencies.

The oscillations at the stable operating conditions differ from those at the aforementioned unstable conditions in the region of HFO-I, in that there is no clear (dominant) peak at any frequency, which corresponds to the characteristics of the noise. The damping factors at the frequencies of $f = 1540$–1850 Hz are of relatively higher values of 7.8–9.0% than those in the region of HFO-I. Higher damping factors indicate weaker resonant oscillation. Thus, the major difference in oscillating behaviors between the HFO-I region

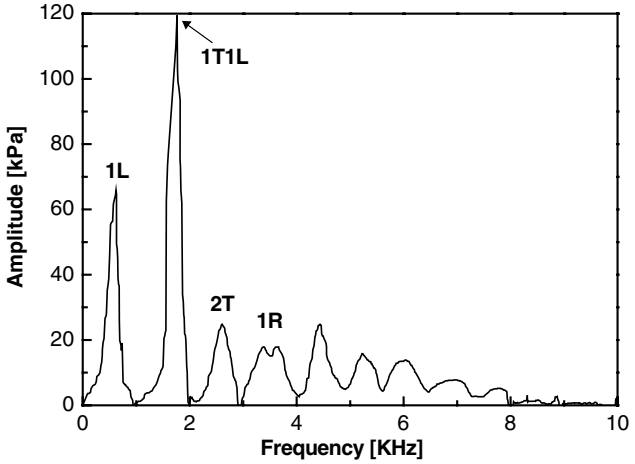

Fig. 5 Typical amplitude spectrum of the injectors with the impingement angle of 30 deg at self-oscillation mode with small amplitude in the lower instability region.

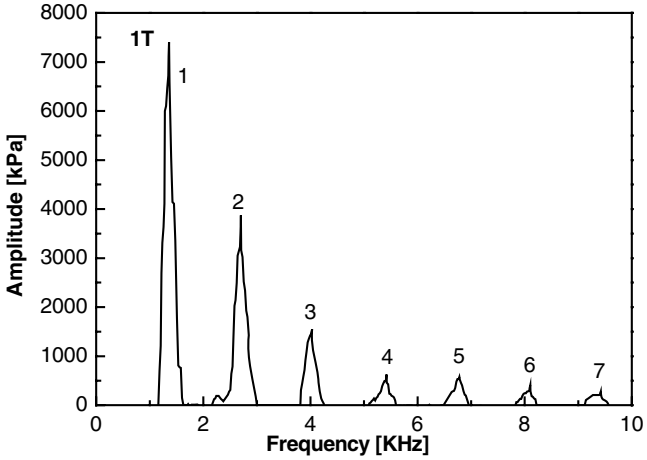

Fig. 6 Typical amplitude spectrum of the injectors with the impingement angle of 30 deg at self-oscillation mode with large amplitude in the upper instability region.

and the stable region lies in the increased damping factor at the peak frequency rather than in the amplitude level at the dominant spectrum frequency.

The upper instability region of HFO-II has values of p_{ch} more than twice as high as those of the operating window as shown in Fig. 4, and the pressure oscillations at a frequency of $f_{1T} = 1650 \pm 250$ Hz are observed in the region. In the present test, the chamber pressure is adjusted by varying the propellant injection velocities, U_O and U_F. The lower part of the region shows the pressure oscillations with small amplitudes as in the right-hand part of HFO-I. However, even by slight subsequent increase in U_O, these small-amplitude oscillations transfer to strong oscillations with large amplitudes up to 7000–9000 kPa. Furthermore, the damping factor is nearly zero: 0.4–1.0%. A representative amplitude spectrum is shown in Fig. 6. The frequency of these oscillations goes down drastically to about 1400 Hz. This remarkable decrease in the frequency can be attributed to the acoustically open end at the outlet of the subscale chamber, which does not have a nozzle. The large acoustic velocity associated with large-amplitude oscillations increases dramatically the intake of cold ambient air into the chamber through its open outlet. As a result, the effective temperature of the combustion products within the subscale combustion chamber decreases, leading to a decrease in the sound speed and the oscillation frequency. A specific feature of the amplitude spectrum for the pressure oscillations of large amplitude in this region is that the frequencies at the dominant peaks are integer multiples of the frequency at the first greatest peak; $f_2 = 2f_1$, $f_3 = 3f_1$, $f_4 = 4f_1$, and so on. As many as seven of these peaks can be counted as shown in Fig. 6. They are harmonics of the fundamental peak and this spectrum pattern has been frequently observed in the case of large-amplitude pressure oscillations in the chamber [21,22].

The lower (HFO-I) and upper (HFO-II) stability boundaries demonstrate that the unstable regions lie outside the operating range. Nevertheless, it can be seen that the left boundary of the operating range is located rather close to the HFO-I region. The stability margin of this region is only 42%. In this case, a pulse or periodic external disturbance in the combustion process may result in transition into the unstable region and give rise to small-amplitude high-frequency oscillations of the tangential modes.

B. Estimation of the Hydrodynamic Lengths of the Impinging Jet Injectors

In the chamber with the jet injectors adopted in this study, the following instability mechanism is suggested: the stability loss is most probable if the characteristic burning time is equal to the acoustic oscillation period, $T = 1/f_{\text{ch}}$ or if there is an integer multiple relationship between these two characteristic times. This is proposed as a necessary condition for triggering the instability. The characteristic time can be estimated by the transport delay of the

propellants from the injector exit to the combustion zone. Accordingly, to verify the instability mechanism, it is required to estimate the characteristic longitudinal length of the combustion zone and then, τ is determined by the equation $\tau = l_{cz}/U_O$. In evaluating τ, the oxidizer injection velocity is selected as the characteristic velocity because the oxidizer mass flow rate is larger than the fuel mass flow rate.

To a first approximation, l_{cz} can be obtained from hydrodynamic calculations involving the use of the dynamic interaction scheme of the oxidizer-fuel jet as shown in Fig. 1b. Assuming that the chemical time scales are much shorter than the mixing time scales (i.e., $\tau_{chem} \ll \tau_{mix}$), we obtain the equality $l_{cz} = l_{mix}$ with good accuracy. For the analysis of the experimental data, the principal characteristic lengths, l_i, should be estimated over a wide range of oxidizer and fuel flow rates.

It follows from the geometric parameters shown in Fig. 1b that the oxidizer and the fuel streams injected separately would join or impinge first at the length, $l_1 = (1.0/\tan\alpha)(4.9 - 0.8/\cos\alpha)$ [mm]. Because of the finite thickness of the jet streams, they would intersect up to the length of $l_2 = (1.0/\tan\alpha)(4.9 + 0.8/\cos\alpha)$ [mm]. These two lengths are determined only by the geometric parameters of the injector irrespective of the operating conditions in the combustion chamber. In the case of $\alpha = 30$ deg, the values of l_1 and l_2 are 6.9 and 10.1 mm, respectively.

The other characteristic lengths of the mixing or combustion zone, l_3, l_4, and l_5, are related to the second impingement point, and the determination of these requires more complex calculations. The following expressions are derived from hydrodynamic calculations:

$$l_3 = \frac{6.0}{\tan\alpha} + \frac{1.9}{\cos(90\ \text{deg} - \alpha)}(1.9q^2 + \cos\alpha)\ [\text{mm}] \qquad (3)$$

$$l_4 = \frac{6.0}{\tan\alpha} + \frac{3.0}{\cos(90\ \text{deg} - \alpha)}(1.9q^2 + \cos\alpha)\ [\text{mm}] \qquad (4)$$

$$l_5 = \frac{6.0}{\tan\alpha} + \frac{4.1}{\cos(90\ \text{deg} - \alpha)}(1.9q^2 + \cos\alpha)\ [\text{mm}] \qquad (5)$$

These calculated values of jet characteristic lengths of l_1 to l_5 are compared with the characteristic lengths measured from flame photographs taken during hot-fire tests in the following section.

C. Flame Behavior and Stability Characteristics

Photographs of the flames were taken to determine the characteristic features of the combustion zone pattern for the stable and the unstable operating conditions of the subscale chamber. The flame was photographed from the direction of view "A" indicated in Fig. 3. Figure 7 shows a photograph and the schematic of the flames produced by the injectors with $\alpha = 30$ deg for one operating condition corresponding to the lower instability region (HFO-I), where $q = 0.41$ and $U_O = 18.5$ m/s. In the schematic, the yellow part of the flame indicates the fuel-rich zone and the blue part indicates the stoichiometric burning zone.

The following notation is adopted in Fig. 7: l_{max} and l_{min} are the distances from the faceplate to the upper and lower boundaries of the intensive flame, respectively. The mean value, l_{mean}, is calculated to be $(l_{max} + l_{min})/2$, and l_{stab} is the distance from the faceplate to the beginning of flame luminance, i.e., the flame stabilization point. And l_x is the shortest distance between the faceplate and the combustion zone with the maximum rate of luminance intensity buildup, i.e., maximum heat release in the zone of fuel jet spreading.

In Fig. 8, the experimental data on the characteristic longitudinal lengths of the combustion zone (l_{max}, l_{min}, l_{mean}, l_x, and L) measured from the photographs taken for various operating conditions are plotted as a function of q for comparison with values obtained through hydrodynamic calculations in the preceding section. The figure shows that the flame stabilization takes place on fuel streams at a distance of $l_{stab} = 3$–4 mm from the faceplate. This distance is shorter than that to the point of initial intersection of the oxidizer and the fuel jet, l_1. This difference between l_{stab} and l_1 is due to the effect of backflows which occur both at the jet-impact point and in the space surrounding the jets.

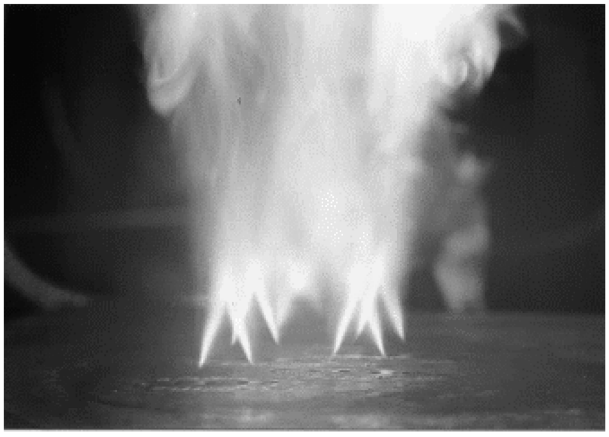

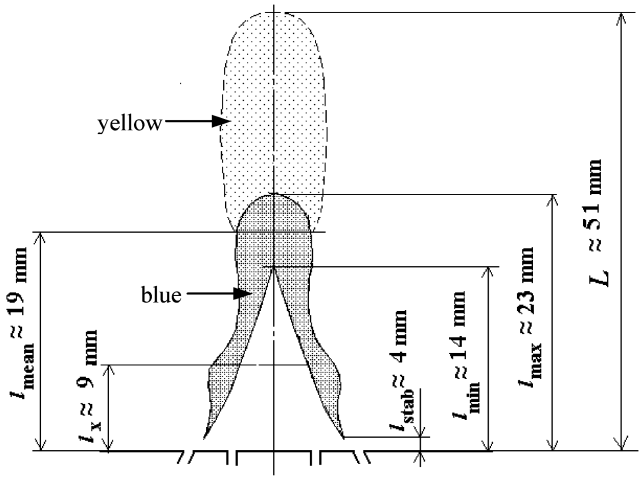

Fig. 7 Photograph and schematic of flames formed by the injectors with the impingement angle of 30 deg for one operating condition in the lower instability region ($q = 0.41$ and $U_O = 18.5$ m/s).

It can be seen from Fig. 8 that in the HFO-I region, the characteristic longitudinal length of the combustion zone, $l_{max} = 19$–23 mm, is close to the distance $l_5 = 19$–20 mm. The

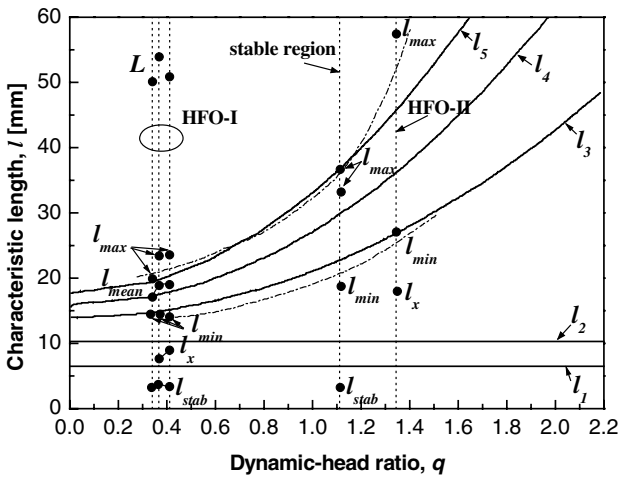

Fig. 8 Calculated and measured characteristic lengths of the injectors with the impingement angle of 30 deg as a function of q (symbol: measured value, solid line: calculated value of each characteristic length, dash-dotted line: curve fitting of l_{min} and l_{max} data).

value of $l_{\min} = 14$ mm is close to the calculated value of $l_3 = 15$ mm. The characteristic length of the combustion zone, $l_{\text{mean}} = 17$–19 mm is close to the calculated value of $l_4 = 17$–18 mm. Finally, the value of $l_x = 8$–9 mm is close to the calculated values of the distances from the injector faceplate to the initial impingement point of the inner and outer surfaces of the fuel jets and the outer surface of the oxidizer jets, i.e., $l_1 = 6.9$ mm and $l_2 = 10.1$ mm in the case of $\alpha = 30$ deg. Values of $L = 50$–54 mm are higher than any other calculated distances.

Accordingly, based on the results of this comparative analysis, all the characteristic lengths of the combustion zone measured from photographs are found to coincide with the calculated values of the distance from the injector faceplate to the impact points; $l_x = l_1$–l_2, $l_{\min} = l_3$, $l_{\text{mean}} = l_4$, and $l_{\max} = l_5$. This finding verifies that the characteristic lengths calculated from hydrodynamics of jets are valid for the chemically reactive conditions, and furthermore, they have an important physical significance in triggering the instability.

As q is increased further up to 2.2 (the maximum value of q), the instability observed in the HFO-I region disappears. Figure 9 shows the photograph and the schematic of the flame produced by the injectors near the nominal operating condition within the stable region, where $q = 1.12$ and $U_O = 24.9$ m/s. Flame photographs, not shown here, demonstrate that the combustion zone pattern changes significantly when q is greater than unity. Compared with the aforementioned case with $q < 1.0$ in the HFO-I region, the combustion zone with $q > 1.0$ is substantially more extended and the flame intensity increases due to the flame's approach to the near-equilibrium condition. The secondary impingement of the bipropellant burning-out streams at nearly nominal (design) operation of the injectors takes place much farther from the injector faceplate (with $l_{\min} = 19$ mm and $l_{\max} = 33$–37 mm, respectively) than at low values of q corresponding to the lower instability region ($l_{\min} = 14$ mm and $l_{\max} = 19$–23 mm, respectively). The disappearance of the HFO-I region at high q is in good agreement with the fact that near-equilibrium flames contribute to the attenuation of pressure oscillation [23,24] and the distributed combustion zone mitigates the acoustic resonance.

In the region of HFO-II, where large-amplitude pressure oscillations are triggered, an unstable behavior distinct from that in the HFO-I region is observed. Figure 10 shows the photograph and the schematic of the flames for one operating condition within the HFO-II region, where $q = 1.35$ and $U_O = 67.5$ m/s. The relatively high velocity of the oxygen stream is worth noting. Furthermore, it is worthy of note that the flame is blue throughout the combustion zone. Also, local zones of intensive luminance (i.e., high heat-release-rate) in the flame of every injector stand out sharply. The distance from the injector faceplate to the beginning of the flame luminance, l_{stab}, is spatially nonuniform and depends on the flame position formed by each of the five-element injectors. These characteristics are similar to those of flames burning under the pre-blowout condition. The measured characteristic lengths of the flame are demonstrated in Fig. 10, which shows an appreciably lifted-off flame. Accordingly, it is worthy of note that the combustion zone pattern formed in the upper instability region is largely governed by the characteristics of pre-blowout combustion.

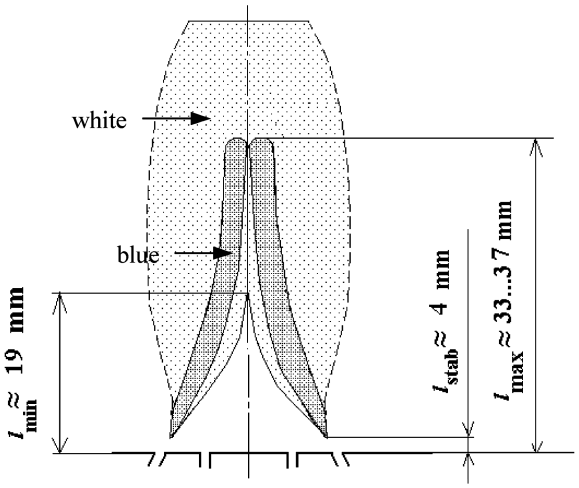

Fig. 9 Photograph and schematic of flames formed by the injectors with the impingement angle of 30 deg for one operating condition in the stable region ($q = 1.12$ and $U_O = 24.9$ m/s).

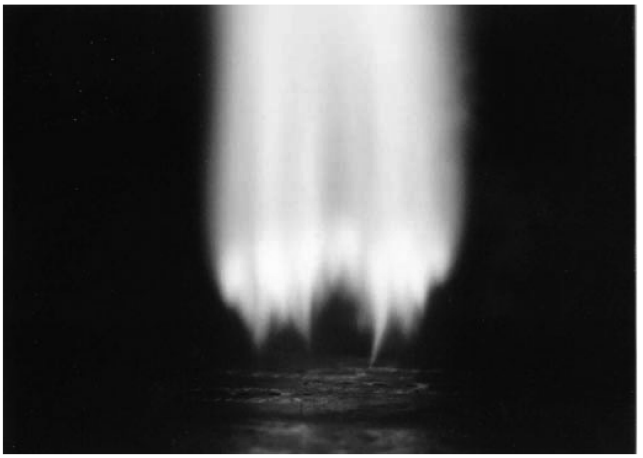

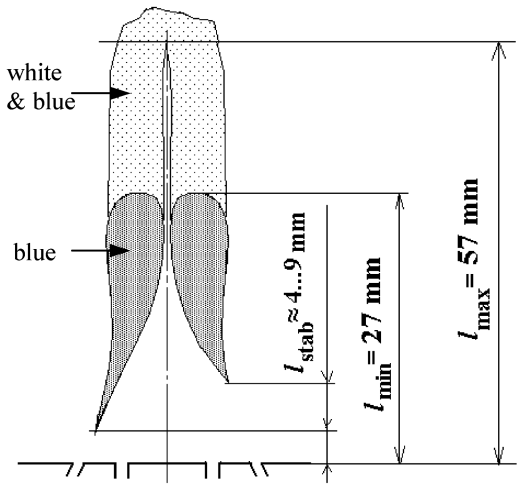

Fig. 10 Photograph and schematic of flames formed by the injectors with the impingement angle of 30 deg for one operating condition in the upper instability region ($q = 1.35$ and $U_O = 67.5$ m/s).

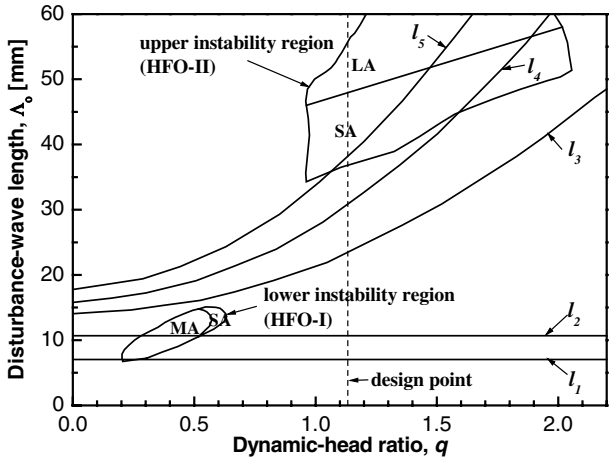

Fig. 11 Stability boundaries plotted on the coordinate plane of disturbance-wave length, Λ_o vs q.

Agreement between the experimental characteristic lengths of the combustion zone measured from the photographs and the corresponding calculated values makes it possible to use the calculated values with good accuracy in the analysis of hot-fire test results. In this context, the correlation of the calculated characteristic lengths of the combustion zone, l_1–l_5, with the parameter $\Lambda_O = U_O/f_{\text{ch}} = U_O T$ is of interest. Λ_O is introduced to indicate the length of a disturbance wave propagating along the oxidizer jet at the jet velocity, U_O. When determining Λ_O, the frequency, f_{ch}, is chosen as follows: for the instability regions I and II, the frequency is taken to be that of the dominant oscillation, whereas for the stable operation the frequency is taken to be that for the major maximum of the amplitude spectra of the in-chamber noise.

The correlation between the experimental data of Λ_O and the calculated values of l_1–l_5 is illustrated as a function of q in Fig. 11. The instability-boundary data can be obtained by the transformation of the data in Fig. 4 onto the Λ_O–q coordinate plane. From this figure, the following points can be found. The lower instability region with small- or medium-amplitude self-excited oscillations, for which the correlation of $\Lambda_O = l_1$–$l_2 = 6.9$–10.1 mm is applicable, can be attributed to an unsteady process of the oxidizer and the fuel jet impingement related to the characteristic disturbance-propagation time along the oxidizer stream, $\tau_O = (l_1$–$l_2)/U_O = 0.40$–0.58 ms. τ_O is the characteristic burning time as discussed in the preceding section. The reciprocal value of this time, $\tau_O^{-1} = U_O/(l_1$–$l_2) =$ 1700–2500 Hz, coincides approximately with the acoustic oscillation frequency within the combustion chamber, $f_{\text{ch}} = f_{1\text{T1L}} =$ 1850 ± 150 Hz. One part of the upper instability region (II) with small-amplitude self-excited oscillations has fundamentally the same instability mechanism as aforementioned. That is, the amplitude of the oscillation increases under favorable phase conditions where the reciprocal value of the transport delay time, $\tau_O^{-1} = U_O/(l_4$–$l_5)$ is close to the acoustic oscillation frequency, $f_{\text{ch}} = f_{1\text{T}}$. The same reasoning is applied to the other part of the upper instability region (II) with large-amplitude oscillations. The only difference is that in the latter case, clouds of unburned combustible mixture move along the combustion zone with a velocity approximately equal to U_O. The clouds are formed as a result of incomplete combustion near the blowout condition. While moving in the downstream direction, these local clouds burn out at distances of l_4 and l_5 from the injector faceplate. As a result, the amplitude of the self-excited oscillations is increased, leading to strong pressure fluctuations.

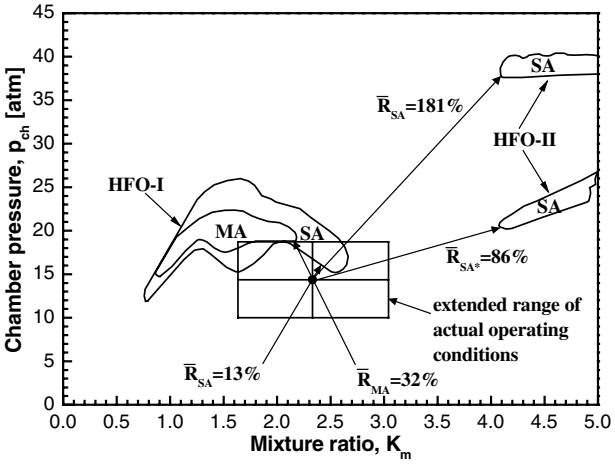

Fig. 12 Stability boundaries and margins of the injectors with the impingement angle of 20 deg plotted on the coordinate plane of chamber pressure vs mixture ratio.

D. Effect of the Impingement Angle on the Stability Margin

With an injector configuration of $\alpha = 20$ deg, the measured instability-region boundaries are shown in Fig. 12. As demonstrated in the figure, two upper instability regions are presented and the stability margin for the lower one is marked by $\bar{R}_*$. The figure shows that the decrease in the impingement angle from $\alpha = 30$ deg to

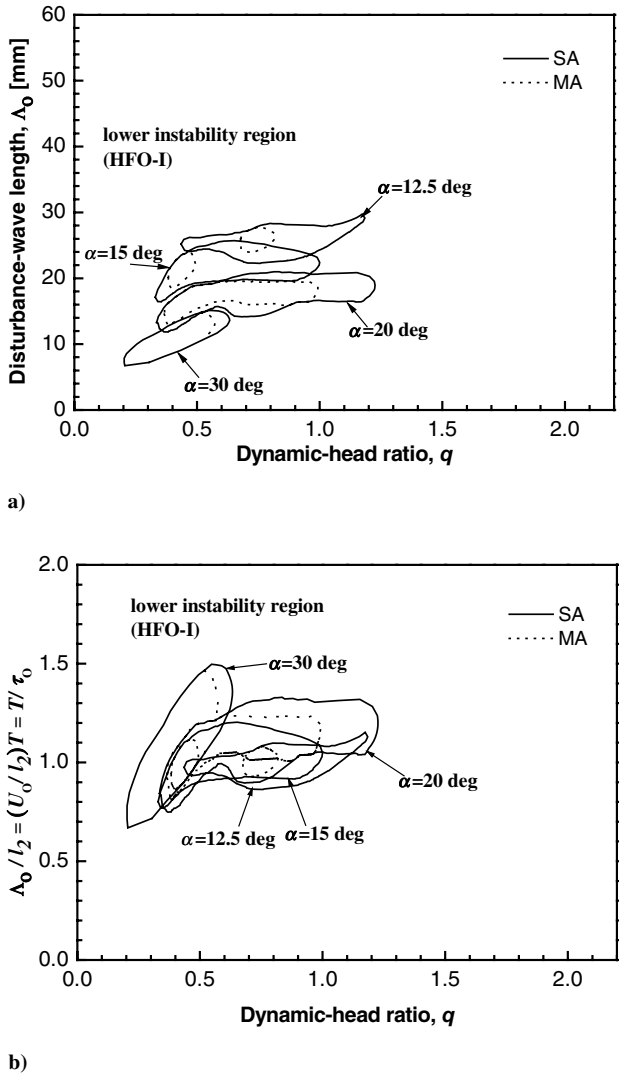

Fig. 13 Stability boundaries of the lower instability region of the injectors with various impingement angles plotted on the coordinate planes of a) disturbance-wave length, Λ_o vs q and b) nondimensionalized parameter of $T/\tau_O = (U_O/l_2)T = \Lambda_O/l_2$ vs q (SA: small amplitude, MA: medium amplitude).

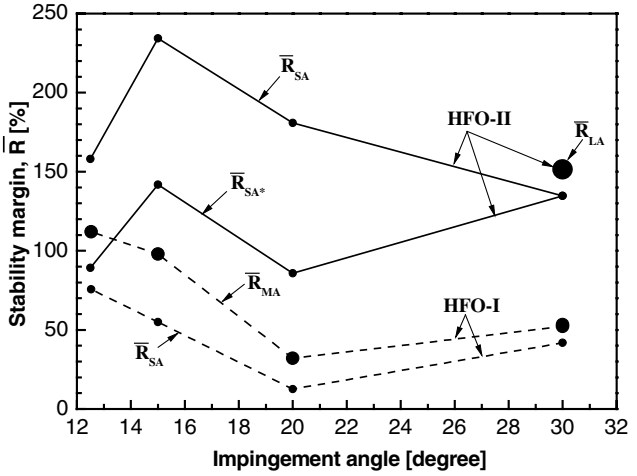

Fig. 14 Stability margins as a function of the impingement angle in the lower (HFO-I) and the upper (HFO-II) instability regions.

$\alpha = 20$ deg adversely affects the combustion stability. The stability margins toward both instability regions I and II have decreased.

The tests were also conducted with the other injector configurations of $\alpha = 15$ and 12.5 deg. They have basically the same instability regions as those of $\alpha = 30$ and 20 deg. As α decreases, the instability-region boundaries shift to a higher pressure regime because the characteristic lengths l_1 to l_5 are increased.

All the HFO-I boundaries from the experiments conducted with all of the impingement angles are shown on the Λ_o–q coordinate plane in Fig. 13a. As α decreases, the unstable regions shift to higher ranges of both Λ_o and q. This shift can be explained as follows. As mentioned in the preceding section, it is found that the stability boundary of HFO-I is closely correlated with the first impingement length, l_2, and triggering of the instability occurs when $\tau_O = l_2/U_O \approx T$. As α increases, the length l_2 decreases and therefore, the oxidizer velocity, U_O, should be increased to maintain a constant value of τ_O for triggering of the instability. The increase in U_O results in the increase in q, as well as the increase in the disturbance-wave length, $\Lambda_O = U_O/f_{\text{ch}} = U_O T$ with T fixed. Based on this analysis, the nondimensional parameter $T/\tau_O = T/(l_2/U_O) = \Lambda_O/l_2$ is introduced for correlation of all the boundary data. That is, all the data on the HFO-I boundary are grouped to normalize T with τ_O. As shown in Fig. 13b, the grouped data show a good correlation between T and τ_O and all the unstable regions of HFO-I are located near the unity value of the new parameter, T/τ_O. This point strongly supports the instability mechanism that triggering of the instability occurs when $\tau_O \approx T$. On the other hand, although not shown here, a weak correlation was observed in the case of HFO-II because the additional effect of the lifted-off flame dynamics is involved in the pressure oscillations and the ambiguous resonant frequencies result from the fluctuating sound speed. These points are predictable from the results shown in Fig. 11.

The stability margins are obtained as a function of α and shown in Fig. 14. When the impingement angle is decreased from $\alpha = 20$ to 15 deg, the stability margin with respect to the nearest instability region I increases dramatically. An increase in the stability margin is also noted with respect to the upper instability region II. With a further decrease in the angle down to $\alpha = 12.5$ deg, the stability margin in relation to the instability region I increases, but decreases in relation to the instability region II. The injector configuration with an impingement angle $\alpha = 20$ deg has the smallest stability margin.

IV. Conclusion

Combustion-instability boundaries have been investigated experimentally with a subscale rocket chamber for screening the injector configurations. The split-triplet impinging jet injectors were employed. With a sample full-scale chamber selected, the subscale chamber was designed using the scaling methods proposed in the previous works to determine the geometrical dimensions and the operating conditions. Hot-fire test procedures were followed to obtain the stability boundaries.

From the experimental tests, two (lower and upper) instability regions were identified using the parameters of combustion chamber pressure and mixture ratio, which are customary for combustor designers. The instability mechanisms are rather complex, and many physical and chemical processes interact to trigger the instability. Nevertheless, it was found that an important instability mechanism in the chamber with the employed jet injectors could be explained by the correlation between the characteristic burning or mixing time and the characteristic acoustic time. In each instability region, the dynamic behavior of the flames was investigated from the photographs taken to verify the characteristic lengths of the jet injectors derived from hydrodynamic theory. From the experimental data, the length of a hydrodynamic disturbance-wave propagating along the oxidizer stream in the lower instability region was found to be characterized by the distances from the injector face to the first impact points of the oxidizer and the fuel streams. The latter parameters were used for the calculation of the characteristic burning or mixing time. All the data on the boundary of the lower instability region were grouped to normalize the characteristic acoustic time with the characteristic burning time. The normalized data show good correlation between these two parameters. This correlation strongly suggests that the instability can be triggered when the characteristic burning time is close to the characteristic acoustic time in the chamber. This is a necessary condition for triggering the instability. Another required condition is a weak flame intensity near the flame extinction point as reported in the literature [23,24]. In the upper instability region, the instability mechanism is valid but with the characteristic lengths to the second impingement points. The large-amplitude pressure oscillations observed in the upper instability region were found to be generated by the liftoff of the flame near the blowout condition. The present results are not limited to the specific chamber, but are valid in any chambers with the similar impinging jet injectors. Stability margins toward the unstable regions were evaluated with several injector configurations. From the comparative analysis, the optimum impingement angle can be identified.

Except for an impingement angle of 20 deg, the lower and the upper instability boundaries obtained here verify that the unstable regions lie outside the operating range of the sample full-scale chamber. Nevertheless, it can be seen that the left boundary of the operating range is located rather close to the lower instability region. Accordingly, a pulse or periodic external disturbance in the combustion process may result in transition into the unstable region and give rise to the occurrence of high-frequency oscillations of the tangential modes.

Acknowledgment

Support for the conduct of this study from the Basic Research Program of Korea Research Council of Public Science and Technology is gratefully acknowledged.

References

[1] Harrje, D. J., and Reardon, F. H. (eds.), "Liquid Propellant Rocket Combustion Instability," NASA SP-194, 1972.

[2] McManus, K. R., Poinsot, T., and Candel, S. M., "A Review of Active Control of Combustion Instabilities," *Progress in Energy and Combustion Science*, Vol. 19, No. 1, 1993, pp. 1–29.

[3] Culick, F. E. C., and Yang, V., "Overview of Combustion Instabilities in Liquid-Propellant Rocket Engines," *Liquid Rocket Engine Combustion Instability*, edited by V. Yang and W. E. Anderson, Vol. 169, Progress in Astronautics and Aeronautics, AIAA, Washington, DC, 1995, pp. 3–37.

[4] Anderson, W. E., Ryan, H. M., and Santoro, R. J., "Combustion Instability Phenomena of Importance to Liquid Bipropellant Rocket Engines," CPIA Publ. 573, Vol. 2, 1991, pp. 99–112.

[5] Muss, J. A., "Instability Phenomena in Liquid Oxygen/Hydrocarbon Rocket Engines," *Liquid Rocket Engine Combustion Instability*, edited by V. Yang and W. E. Anderson, Vol. 169, Progress in Astronautics and Aeronautics, AIAA, Washington, DC, 1995, pp. 73–88.

[6] Kim, J. S., and Williams, F. A., "Acoustic-Instability Boundaries in

Liquid Propellant Rockets: Theoretical Explanation of Empirical Correlation," *Journal of Propulsion and Power*, Vol. 12, No. 3, 1996, pp. 621–624.

[7] Anderson, W. E., Ryan, H. M., Santoro, R. J., and Hewitt, R. A., "Combustion Instability Mechanism in Liquid Rocket Engines Using Impinging Jet Injectors," AIAA Paper 95-2357, July 1995.

[8] Blomshield, F. S., Crump, J. E., Mathes, H. B., and Stalnaker, R. A., "Stability Testing of Full-Scale Tactical Motors," *Journal of Propulsion and Power*, Vol. 13, No. 3, 1997, pp. 349–355.

[9] Blomshield, F. S., Mathes, H. B., Crump, J. E., and Beiter, C. A., "Nonlinear Stability Testing of Full-Scale Tactical Motors," *Journal of Propulsion and Power*, Vol. 13, No. 3, 1997, pp. 356–366.

[10] Kim, H. J., Lee, K. J., Seo, S., Han, Y. M., Seol, W. S., and Lee, S. Y., "Stability Rating Tests of KSR-III Baffled Chamber Using Pulse Gun," AIAA Paper 2004-3364, July 2004.

[11] Fisher, S. C., Dodd, F. E., and Jensen, R. J., "Scaling Techniques for Liquid Rocket Combustion Stability Testing," *Liquid Rocket Engine Combustion Instability*, edited by V. Yang and W. E. Anderson, Vol. 169, Progress in Astronautics and Aeronautics, AIAA, Washington, DC, 1995, pp. 545–564.

[12] Dexter, C. E., Fisher, M. F., Hulka, J. R., Denisov, K. P., Shibanov, A. A., and Agarkov, A. F., "Scaling Techniques in Liquid Rocket Engine Combustion Devices Testing," *The Second International Symposium on Liquid Rocket Engines*, ONERA, Paris, 1995.

[13] Sohn, C. H., Seol, W. S., Shibanov, A. A., and Pikalov, V. P., "On the Method for Hot-Fire Modeling of High-Frequency Combustion Instability in Liquid Rocket Engines," *KSME International Journal*, Vol. 18, No. 6, 2004, pp. 1010–1018.

[14] Huzel, D. K., and Huang D. H., *Modern Engineering for Design of Liquid-Propellant Rocket*, Vol. 147, Progress in Astronautics and Aeronautics, AIAA, Washington, DC, 1992, p. 35.

[15] Gill, G. S., and Nurick, W. H., "Liquid Rocket Engine Injectors," NASA SP-8089, 1976.

[16] Sutton, G. P., *Rocket Propulsion Elements*, 6th ed., John Wiley & Sons, New York, 1992, Chap. 10.

[17] Laudien, E., Pongratz, R., Pierro, R., and Preclik, D., "Experimental Procedures Aiding the Design of Acoustic Cavities," *Liquid Rocket Engine Combustion Instability*, edited by V. Yang, and W. E. Anderson, Vol. 169, Progress in Astronautics and Aeronautics, AIAA, Washington, DC, 1995, pp. 377–399.

[18] Zucrow, M. J., and Hoffman, J. D., *Gas Dynamics*, Vol. 2, John Wiley & Sons, New York, 1977, Chap. 15.

[19] Natanzon, M. S., *Combustion Instability*, Mashinostroyeniye, Moscow, 1986, Chap. 3.

[20] Sohn, C. H., Seol. W. S., Lee, S. Y., Kim, Y.-M., and Lee, D. S., "Application of Combustion Stabilization Devices to Liquid Rocket Engine," *Journal of The Korean Society for Aeronautical and Space Sciences* (in Korean), Vol. 31, No. 6, 2003, pp. 79–87.

[21] Przekwas, A. J., and Yang, H. Q., "Advanced CFD Methodology for Fast Transients Encountered in Nonlinear Combustion Instability Problem," CFDRC Rept. 4065/1 Under Contract No. NAS8-38034, Marshall Space Flight Center, AL, 1989.

[22] Kinsler, L. E., Frey, A. R., Coppens, A. B., and Sanders, J. V., *Fundamentals of Acoustics*, 4th ed., John Wiley & Sons, New York, 2000, Chap. 2.

[23] Kim, J. S., and Williams, F. A., "Contribution of Strained Diffusion Flames to Acoustic Pressure Response," *Combustion and Flame*, Vol. 98, No. 3, 1994, pp. 279–299.

[24] Sohn, C. H., Chung, S. H., Kim, J. S., and Williams, F. A., "Acoustic Response of Droplet Flames to Pressure Oscillations," *AIAA Journal*, Vol. 34, No. 9, 1996, pp. 1847–1854.

T. Lieuwen
Associate Editor